

Topological insulator Bi_2Se_3 films on rare earth iron garnets and their high-quality interfaces

C. C. Chen (陳俊嘉),¹ K. H. M. Chen (陳可璇),¹ Y. T. Fanchiang (范姜宇廷),² C. C. Tseng (曾俊智),¹ S. R. Yang (楊尚融),¹ C. N. Wu (巫啓男),¹ M. X. Guo (郭孟鑫),¹ C. K. Cheng (鄭兆凱),² C. T. Wu (吳建霆),³ M. Hong (洪銘輝),^{2, a)} and J. Kwo (郭瑞年)^{1, a)}

¹*Department of Physics, National Tsing Hua University, Hsinchu 30013, Taiwan*

²*Department of Physics, National Taiwan University, Taipei 10617, Taiwan*

³*National Nano Device Laboratories, Hsinchu 30013, Taiwan*

a) To whom the correspondence is addressed: raynien@phys.nthu.edu.tw (J. Kwo) and mhong@phys.ntu.edu.tw (M. Hong)

Abstract

The integration of quantum materials like topological insulators (TIs) with magnetic insulators (MIs) has important technological implications for spintronics and quantum computing. Here we report excellent crystallinity of c-axis oriented epitaxial TI films Bi_2Se_3 grown on MI films, a rare earth iron garnet (ReIG), such as thulium iron garnet ($\text{Tm}_3\text{Fe}_5\text{O}_{12}$, TmIG) by molecular beam epitaxy (MBE) with a Se-buffered low-temperature (SBLT) growth technique. We demonstrated a streaky reflection high-energy electron diffraction pattern starting from the very first quintuple layer of Bi_2Se_3 , indicating the high-quality interface between TmIG and Bi_2Se_3 , a prerequisite for studying interfacial exchange coupling effects. The strong interfacial exchange interaction was manifested by observations of anomalous Hall effect in the Bi_2Se_3 /TmIG bilayer and a shift of ferromagnetic resonance field of TmIG induced by Bi_2Se_3 . We have reproducibly grown high-quality Bi_2Se_3 /ReIG and interfaces using this new TI growth method, which may be applied to grow other types of van der Waals (vdW) hetero-structures.

Topological insulators (TIs) have attracted great interests in the field of condensed matter sciences because of the exotic topological edge or surface state (TSS) arising from the bulk band inversion driven by strong spin-orbit coupling (SOC).¹ The electrons at the surface state are protected by time reversal symmetry (TRS), and the spin-momentum locking feature has led to a transport forbidding back-scattering.² A series of three-dimensional (3D) TIs with a single Dirac cone at Γ point of momentum spaces, such as Bi_2Se_3 , Bi_2Te_3 , and Sb_2Te_3 , were discovered and received feverish studies in the past decade.^{3,4} Recently, research interests have turned to the phenomena emerging from broken TRS in ferromagnetic TIs. Quantum anomalous Hall effect (QAHE), the latest member of the Hall family, exhibits a quantized Hall conductivity $\sigma = \frac{e^2}{h}$ without any external magnetic field, and generates exciting new physics to be explored in the ferromagnetic TI systems.⁵ The dissipationless chiral transport in QAH states displays high potential in the development of spin transport devices with low-power consumption.^{6,7} Although QAHE was demonstrated in magnetically doped TI systems, the QAH regime is restricted to be below 2 K.^{8,9} In addition, extra carriers and inevitable crystal defects were generated by excess dopants in the films, which may destroy novel quantum states.¹⁰

An alternative way to introduce ferromagnetism in the TI is to couple the TI with a magnetic insulator (MI), thereby inducing a magnetic order through magnetic proximity effect (MPE). Compared to the samples with magnetic doping, a more uniform magnetization without crystal defects may be developed in the hetero-structures under MPE. The ferromagnetic insulators are preferred over ferromagnetic metals to ensure a clean interface, avoiding chemical interaction and current shunting. A TI/MI hetero-structure with a small lattice mismatch was first demonstrated in $\text{Bi}_2\text{Se}_3/\text{EuS}$.¹¹ The

epitaxial growth has resulted in the persistence of MPE to room temperature, suggesting that much stronger exchange field can be generated to break TRS.¹² However, the low Curie temperature (T_c) ~ 17 K and the preferred in-plane shape anisotropy of EuS thin films precluded a large out-of-plane magnetization in absence of magnetic fields for practical applications.

In contrast, ferrimagnetic rare earth iron garnets (ReIGs) of high T_c above 500 K may be an attractive choice. Thulium iron garnet ($\text{Tm}_3\text{Fe}_5\text{O}_{12}$ (TmIG)) exhibiting perpendicular magnetic anisotropy (PMA) is preferred over the well-known yttrium iron garnet ($\text{Y}_3\text{Fe}_5\text{O}_{12}$ (YIG)) with in-plane anisotropy (IMA). To grow high-quality TI thin films on ReIG substrates, however, is challenging, since the large lattice mismatch and the complicated atomic arrangement on the garnet surface have posed difficulties in developing a sharp interface, the prerequisite to establish a direct coupling effect between TSS and MI. In most cases, an interlayer with poor crystallinity formed in TI/ReIG bilayers,¹³⁻¹⁶ which would greatly suppress the interfacial coupling. This, however, is inevitable if the TI films were grown by using the conventional two-step method.¹⁷ Although an MPE above 400 K has been recently demonstrated in $(\text{Bi,Sb})_2\text{Te}_3/\text{TmIG}$,¹⁸ the TI/ReIG interface quality showed notable variations, leading to a large fluctuation of MPE properties and hampering further systematic studies.^{16,19} Therefore, it is of utmost importance to establish a robust experimental procedure to consistently obtain high-quality TI/ReIG samples.

Here, we have developed a new MBE growth method to overcome the large lattice mismatch in the TI/MI hetero-structures, enabling excellent crystallinities at the hetero-interface and the bulk of TI. Our method has *reproducibly* produced high-quality $\text{Bi}_2\text{Se}_3/\text{TmIG}$ hetero-structures, with an

atomically sharp interface. The MBE-grown Bi₂Se₃ thin films were deposited on tensile-strained TmIG films of PMA^{20,21} with a high T_c ~560 K, which is expected to fulfill the low-power-dissipation magnetization switching.²² The Bi₂Se₃/TmIG thin films with a sharp interface showed excellent crystallinity characterized by several structural analyses. Hysteresis loops were observed in low temperature magnetoresistance (MR), which may correspond to anomalous Hall effect (AHE) coming from the magnetized interface on the TI side, or efficient spin transfer at the interface analogous to the spin Hall magnetoresistance (SMR) observed in heavy metal/MI.²³ Moreover, a large shift of the ferromagnetic resonance (FMR) field was observed, indicating a change of magnetic anisotropy induced by TI. The structural perfectness has contributed to clear observations of the strong interfacial exchange coupling at the TI/MI interface. This has enabled us to further investigate MPE and spin-transfer mechanism in TI/MI structures, where MI may include TmIG, YIG, and Fe₃O₄²⁴, etc. Furthermore, similar growth can be applied to other 2D materials with van der Waals (vdW) bonding to substrates.

The TmIG films were grown on gadolinium gallium garnet (Gd₃Ga₅O₁₂ (GGG)) substrates by off-axis sputtering.^{20,21} The TmIG films were *ex-situ* transferred into the MBE system immediately after they were loaded out from the sputtering chamber. Our MBE system has a base pressure around 4×10^{-10} Torr with high-purity (99.9999%) Bi and Se sources in standard effusion cells. Bright and clear reflection high-energy electron diffraction (RHEED) patterns of TmIG (111) after outgassing the sample at 150 °C indicated the attainment of a high degree of crystallinity and smooth surface, ensuring the growth of high-quality hetero-structures (Fig. 1(a)). The growth rate of our Bi₂Se₃ films

is 0.3 - 0.4 nm/min and the ratio of Se/Bi flux for the growth is 5. Before the growth of TI films, the garnet surface was first covered by an amorphous Se buffer layer ~ 2 nm thick, followed by an amorphous $\text{Bi}_x\text{Se}_{1-x}$ layers ~ 1 nm thick at 50°C . As the substrate temperature ascended to 250°C , the amorphous mixture of $\text{Bi}_x\text{Se}_{1-x}$ crystallized and exhibited streaky Bi_2Se_3 RHEED patterns, revealing an excellent crystallinity of the first quintuple layer (QL) forming at the interface (Fig. 1(b)).

In sharp contrast, using the conventional two-step growth procedure, spotted ring RHEED features of the first QL indicated polycrystalline Bi_2Se_3 domains with a rough surface forming at the interface (Fig. 1(e)). The complicated atomic arrangement of garnet surface prevented Bi and Se atoms from stacking orderly on such surface. The distinct difference revealed at the first QL between the two different growth methods showed that the crystallinity of the initial layer was significantly improved by our new growth technique, which is crucial for fabricating TI/MI hetero-structures.

The Se buffer layer is key to the initiation of the crystallization process of Bi_2Se_3 , which would otherwise be hampered by the lattice-mismatched substrate hosting dangling bonds. The Se buffer layer was covered merely by about 1 nm thick Bi_2Se_3 . It is conceivable that the excess Se of the buffer layer evaporated away as the substrate temperature was raised to 250°C , leaving a well crystalized ~ 1 nm Bi_2Se_3 which became an ideal template for the rest of film growth (Fig. 2(c)). The absence of excess Se was further confirmed by our high-resolution transmission electron microscope (HRTEM) image in Fig. 3. The effect of the Se buffer layer thickness on the quality of the first QL of Bi_2Se_3 was also investigated, and the results are given in the Supplemental Material.

More distinct RHEED patterns of Bi_2Se_3 films in further growth by our recipe have shown that

the crystallinity of Bi_2Se_3 were steadily enhanced during the entire growth (Fig. 1(c), (d)). Very bright RHEED patterns were obtained toward the end of the growth. On the other hand, for the two-step growth, the 2D line features did not show up among the rings until the 3rd QL (Fig. 1(f)). The line features finally took over, leading to streaky RHEED patterns at the 7th QL (Fig. 1(g)). From the evolution of RHEED patterns, the grains began to enlarge at the 3rd QL and started to form a smoother 2D surface. In contrast to the two-step growth, the streaky RHEED of the 1st QL using our growth technique is evidenced for a well ordered atomic arrangement at the interface, which is required to form a strong coupling of the Bi_2Se_3 bottom surface with the MI underneath. Hereafter, we refer our new growth procedure as "Se-buffered low-temperature" (SBLT) growth. In addition, two different diffraction spacing, $[11\bar{2}0]$ and $[1\bar{1}00]$, existed together in the RHEED patterns of Bi_2Se_3 , which have also been observed in previous works of TIs grown on garnet structures.^{13-15,18,19,25} The intensities of streaks were almost the same in all in-plane angles, corresponding to domains randomly oriented azimuthally on the surface. Moreover, the X-ray diffraction (XRD) results on the SBLT-grown Bi_2Se_3 films (in the Supplemental Material) showed no orientation relationship with regard to the substrate, implying that the Bi_2Se_3 domains at the interface crystallized by themselves instead of epitaxially grew on the substrate. The overall SBLT growth process is illustrated graphically in Fig. 2(a)-(d), and the distinct difference in surface morphologies between the films grown by the SBLT and the conventional two-step methods is given in the Supplemental material.

We further characterized the interfacial atomic stacking of $\text{Bi}_2\text{Se}_3/\text{TmIG}$ using HRTEM. Figure 3 shows the layered structure of Bi_2Se_3 , where each QL is comprised of Se-Bi-Se-Bi-Se atomic sequence.

As visualized from the interface, the stacking feature emerged from the first QL is without an extra layer, providing direct evidence that virtually no extra Se atoms, if any, remained after the sample was annealed at 250 °C. Further, we have employed high-angle annular dark-field (HAADF) imaging using Cs-corrected STEM to give the interface atomic arrangement with a higher resolution. As shown in the inset of Fig. 3, a darker interfacial layer, presumably the first QL of Bi₂Se₃, was observed, which exhibits a similar crystal structure as the well-crystallized part of the Bi₂Se₃ film. The Bi₂Se₃-like structure may evolve from the Bi_xSe_{1-x} seed layer and containing smaller crystal domains compared to those in the following QLs. In addition, at the initial growth stage a Se buffer was used to suppress direct chemical bonds between Bi₂Se₃ and TmIG to promote vdW epitaxy. The re-evaporation of the Se buffer layer and the annealing to 250 °C potentially modified the chemical environment, which may enhance the interfacial bonding and diminish the vdW nature of the first QL. In such a scenario, the first QL acts as a transition layer to connect the 2D (Bi₂Se₃) and 3D (TmIG) structures.²⁶ True vdW epitaxy can be realized when the substrate is of layered structure such as graphene, monolayer MoS₂ or In₂Se₃.²⁷⁻²⁹ However, our study suggests that, for a non-vdW type substrate, a transition layer may be necessary for obtaining a high-quality TI-based hetero-structure.

Electrical transport measurements on the Bi₂Se₃/TmIG bilayer were conducted. In Fig. 4(a), we observed the feature of AHE: a clear hysteresis loop in the Hall resistance (R_{xy}) after subtracting the ordinary Hall effect background of the Bi₂Se₃/TmIG. The coercive field H_c of the hysteresis loop increased as the temperature decreased, while the AHE amplitude R_{AHE} was weakly temperature dependent from 50 K to 220 K. Above 220 K, a hysteresis loop signal was too small to detect due to

an insufficient signal-to-noise ratio. The increasing H_c toward low temperature might be associated with the strengthened PMA of TmIG films because of the increasing film strains at low temperatures.³⁰ There are two possible origins of the AHE signals. Firstly, if the Bi_2Se_3 bottom surface was magnetized by MPE, the induced magnetization would contribute to the R_{xy} . We note that the temperature dependence of R_{AHE} for our $\text{Bi}_2\text{Se}_3/\text{TmIG}$ is distinct from the earlier work,²⁵ where the R_{AHE} of $(\text{Bi}_{0.16}\text{Sb}_{0.84})_2\text{Te}_3/\text{YIG}$ decreased with increasing temperature and vanished at 150 K. Moreover, robust AHE loops persisting up to 400 K were reported in $(\text{Bi,Sb})_2\text{Te}_3/\text{TmIG}$.¹⁸ The different T dependence of R_{AHE} of our $\text{Bi}_2\text{Se}_3/\text{TmIG}$ films was attributed to the bulk states of Bi_2Se_3 being conductive, where the transport properties of the magnetized TI may entangle with the bulk carriers and hence the contribution from the interface was suppressed. The second possible mechanism of the AHE is based on the spin current transport in Bi_2Se_3 . An applied charge current in Bi_2Se_3 can generate spin accumulation at the interface by spin Hall effect in the bulk or Rashba-Edelstein effect of the surface states. Such non-equilibrium spins would modulate the conductance of TI films if efficient spin-transfer occurs at the interface.³¹ Nonetheless, both MPE and spin transfer at the interface originate from the interfacial exchange coupling, and the observation of AHE attests to the high quality of our $\text{Bi}_2\text{Se}_3/\text{TmIG}$ sample.

As an independent probe of the interfacial effect, FMR measurements were performed to look into the magnetization dynamics of TmIG under the influence of Bi_2Se_3 . Figure 4(b) and (c) compare the resonance field (H_{res}) of bare TmIG and $\text{Bi}_2\text{Se}_3(7 \text{ nm})/\text{TmIG}$ prepared by the two-step method and the SBLT growth method under an in-plane external field. A clear negative shift of H_{res} is observed

after the growth of Bi_2Se_3 layer, and in particular, the H_{res} induced by the Bi_2Se_3 film grown by the SBLT method in Fig. 4(c) is almost three times larger than that presented in Fig. 4(b). The negative shift of H_{res} corresponds to an enhanced IMA at the interface as reported in our previous work on $\text{Bi}_2\text{Se}_3/\text{YIG}$.¹⁵ Based on the study, the magnetization dynamics of TmIG was likely profoundly affected by the TSS of Bi_2Se_3 . The magnetization dynamics modulated by Bi_2Se_3 can thus be viewed as a consequence of strong interfacial exchange coupling as well as spin-momentum locking of TSS.¹⁶ Note that, despite that $\text{Bi}_2\text{Se}_3/\text{TmIG}$ exhibits strain-induced PMA from the bulk of TmIG, Bi_2Se_3 still induces a large interfacial IMA, representing an intensive interfacial exchange interaction existing in the $\text{Bi}_2\text{Se}_3/\text{TmIG}$ bilayer prepared by the SBLT method.

In conclusion, we have invented a new SBLT growth method of attaining high-quality Bi_2Se_3 thin films on ReIG by adding an ultrathin Se buffer layer prior to the Bi_2Se_3 deposition. Corroborated by extensive structural analyses, the Se buffer effectively isolated the crystallization process of Bi_2Se_3 from the rather complicated atomic structure of the ReIG surface, and initiated the layered structure of Bi_2Se_3 film at the very first QL. The excellent crystallinity of the interfacial layer is essential to give high-quality growth for thicker Bi_2Se_3 films. This is testified by the observation of clear AHE in $\text{Bi}_2\text{Se}_3/\text{TmIG}$ prepared by the SBLT growth. Although the physical origin of the AHE by MPE or spin current transport remains to be clarified, both mechanisms pointed to the existence of an enhanced interfacial exchange coupling. An independent evaluation of the enhanced exchange coupling by means of FMR has observed notably larger in-plane magnetic anisotropy in better-quality of Bi_2Se_3 , manifested as a shift of ferromagnetic resonance field compared to that of bare TmIG. Lastly, it is

noteworthy that the new method of growing Bi_2Se_3 can be further extended to other TIs of similar crystal-chemical properties such as Bi_2Te_3 and bulk insulating $(\text{Bi,Sb})_2\text{Te}_3$, and even other type of layered material suitable for vdW epitaxy.

Acknowledgement

The authors would like to thank J. S. Wei for the technical support in transport measurements. Technical support from the Nano group Public Laboratory, Institute of Physics, Academia Sinica in Taiwan is acknowledged. This work was supported by the Ministry of Science and Technology, Taiwan, with grant numbers MOST 105-2112-M-007-014-MY3, 106-2112-M-002-010-, and 106-2622-8-002-001.

References

- 1 L. Fu and C. L. Kane, *Phys. Rev. B* **76** (4), 045302 (2007).
- 2 S.-Y. Xu, Y. Xia, L. A. Wray, S. Jia, F. Meier, J. H. Dil, J. Osterwalder, B. Slomski, A. Bansil, H. Lin, R. J. Cava, and M. Z. Hasan, *Science* **332** (6029), 560 (2011).
- 3 M. Z. Hasan and C. L. Kane, *Rev. of Mod. Phys.* **82** (4), 3045 (2010).
- 4 H. Zhang, C.-X. Liu, X.-L. Qi, X. Dai, Z. Fang, and S.-C. Zhang, *Nat. Phys.* **5** (6), 438 (2009).
- 5 C.-Z. Chang and M. Li, *Journal of physics. Condensed matter : an Institute of Physics journal* **28** (12), 123002 (2016).
- 6 A. Roth, C. Brüne, H. Buhmann, L. W. Molenkamp, J. Maciejko, X.-L. Qi, and S.-C. Zhang, *Science* **325** (5938), 294 (2009).
- 7 C.-Z. Chang, W. Zhao, D. Y. Kim, P. Wei, J. K. Jain, C. Liu, M. H. W. Chan, and J. S. Moodera, *Phys. Rev. Lett.* **115** (5), 057206 (2015).
- 8 C.-Z. Chang, J. Zhang, X. Feng, J. Shen, Z. Zhang, M. Guo, K. Li, Y. Ou, P. Wei, L.-L. Wang, Z.-Q. Ji, Y. Feng, S. Ji, X. Chen, J. Jia, X. Dai, Z. Fang, S.-C. Zhang, K. He, Y. Wang, L. Lu, X.-C. Ma, and Q.-K. Xue, *Science* **340** (6129), 167 (2013).

- 9 C.-Z. Chang, W. Zhao, D. Y. Kim, H. Zhang, B. A. Assaf, D. Heiman, S.-C. Zhang, C. Liu, M. H. W. Chan, and J. S. Moodera, *Nat. Mater.* **14**, 473 (2015).
- 10 M. Liu, J. Zhang, C.-Z. Chang, Z. Zhang, X. Feng, K. Li, K. He, L.-l. Wang, X. Chen, X. Dai, Z. Fang, Q.-K. Xue, X. Ma, and Y. Wang, *Phys. Rev. Lett.* **108** (3), 036805 (2012).
- 11 P. Wei, F. Katmis, B. A. Assaf, H. Steinberg, P. Jarillo-Herrero, D. Heiman, and J. S. Moodera, *Phys. Rev. Lett.* **110** (18), 186807 (2013).
- 12 F. Katmis, V. Lauter, F. S. Nogueira, B. A. Assaf, M. E. Jamer, P. Wei, B. Satpati, J. W. Freeland, I. Eremin, D. Heiman, P. Jarillo-Herrero, and J. S. Moodera, *Nature* **533**, 513 (2016).
- 13 Z. Jiang, C.-Z. Chang, C. Tang, J.-G. Zheng, J. S. Moodera, and J. Shi, *AIP Adv.* **6** (5), 055809 (2016).
- 14 H. Wang, J. Kally, J. S. Lee, T. Liu, H. Chang, D. R. Hickey, K. A. Mkhoyan, M. Wu, A. Richardella, and N. Samarth, *Phys. Rev. Lett.* **117** (7), 076601 (2016).
- 15 Y. T. Fanchiang, K. H. M. Chen, C. C. Tseng, C. C. Chen, C. K. Cheng, S. R. Yang, C. N. Wu, S. F. Lee, M. Hong, and J. Kwo, *Nat. Commun.* **9** (1), 223 (2018).
- 16 C. Tang, Q. Song, C.-Z. Chang, Y. Xu, Y. Ohnuma, M. Matsuo, Y. Liu, W. Yuan, Y. Yao, J. S. Moodera, S. Maekawa, W. Han, and J. Shi, *Sci. Adv.* **4** (6), eaas8660 (2018).
- 17 N. Bansal, Y. S. Kim, E. Edrey, M. Brahlek, Y. Horibe, K. Iida, M. Tanimura, G.-H. Li, T. Feng, H.-D. Lee, T. Gustafsson, E. Andrei, and S. Oh, *Thin Solid Films* **520** (1), 224 (2011).
- 18 C. Tang, C.-Z. Chang, G. Zhao, Y. Liu, Z. Jiang, C.-X. Liu, M. R. McCartney, D. J. Smith, T.

- Chen, J. S. Moodera, and J. Shi, *Sci. Adv.* **3** (6), e1700307 (2017).
- 19 Z. Jiang, C.-Z. Chang, M. R. Masir, C. Tang, Y. Xu, J. S. Moodera, A. H. MacDonald, and Jing Shi, *Nat. Commun.* **7**, 11458 (2016).
- 20 C. N. Wu, C. C. Tseng, Y. T. Fanchiang, C. K. Cheng, K. Y. Lin, S. L. Yeh, S. R. Yang, C. T. Wu, T. Liu, M. Wu, M. Hong, and J. Kwo, *Sci. Rep.* **8** (1), 11087 (2018).
- 21 C. N. Wu, C. C. Tseng, K. Y. Lin, C. K. Cheng, S. L. Yeh, Y. T. Fanchiang, M. Hong, and J. Kwo, *AIP Adv.* **8** (5), 055904 (2018).
- 22 C. O. Avci, A. Quindeau, C.-F. Pai, M. Mann, L. Caretta, A. S. Tang, M. C. Onbasli, C. A. Ross, and G. S. D. Beach, *Nat. Mater.* **16**, 309 (2016).
- 23 H. Nakayama, M. Althammer, Y. T. Chen, K. Uchida, Y. Kajiwara, D. Kikuchi, T. Ohtani, S. Geprägs, M. Opel, S. Takahashi, R. Gross, G. E. W. Bauer, S. T. B. Goennenwein, and E. Saitoh, *Phys. Rev. Lett.* **110** (20), 206601 (2013).
- 24 C. N. Wu et al, private communications (2018).
- 25 Z. Jiang, C. Z. Chang, C. Tang, P. Wei, J. S. Moodera, and J. Shi, *Nano Lett.* **15** (9), 5835 (2015).
- 26 J.-Y. Hwang, Y.-M. Kim, K. H. Lee, H. Ohta, and S. W. Kim, *Nano Lett.* **17** (10), 6140 (2017).
- 27 C.-L. Song, Y.-L. Wang, Y.-P. Jiang, Y. Zhang, C.-Z. Chang, L. Wang, K. He, X. Chen, J.-F. Jia, Y. Wang, Z. Fang, X. Dai, X.-C. Xie, X.-L. Qi, S.-C. Zhang, Q.-K. Xue, and X. Ma, *Appl. Phys. Lett.* **97** (14), 143118 (2010).

- 28 K. H. M. Chen, H. Y. Lin, S. R. Yang, C. K. Cheng, X. Q. Zhang, C. M. Cheng, S. F. Lee, C. H. Hsu, Y. H. Lee, M. Hong, and J. Kwo, *Appl. Phys. Lett.* **111** (8), 083106 (2017).
- 29 N. Koirala, M. Brahlek, M. Salehi, L. Wu, J. Dai, J. Waugh, T. Nummy, M.-G. Han, J. Moon, Y. Zhu, D. Dessau, W. Wu, N. P. Armitage, and S. Oh, *Nano Lett.* **15** (12), 8245 (2015).
- 30 A. Quindeau, C. O. Avci, W. Liu, C. Sun, M. Mann, A. S. Tang, M. C. Onbasli, D. Bono, P. M. Voyles, Y. Xu, J. Robinson, G. S. D. Beach, and C. A. Ross, *Adv. Electron. Mater.* **3** (1), 1600376 (2017).
- 31 Y. Lv, J. Kally, D. Zhang, J. S. Lee, M. Jamali, N. Samarth, and J.-P. Wang, *Nat. Commun.* **9** (1), 111 (2018).

Figure captions

Fig. 1 RHEED patterns of (a) TmIG(111) surface; after growing (b) 1 QL; (c) 3 QL; (d) 7 QL of Bi_2Se_3 with a thin Se buffer layer; after growing (e) 1 QL; (f) 3 QL; (g) 7 QL of Bi_2Se_3 by two-step method.

Fig. 2 Illustrations for the SBLT growth. (a) First covering a Se buffer layer ~ 2 nm thick on TmIG; (b) Depositing ~ 1 nm amorphous mixture of Bi and Se; (c) Bi_2Se_3 seed layer crystallizing and excess Se evaporating during the substrate temperature increasing; (d) Further growth of Bi_2Se_3 films on the seed layer.

Fig. 3 HRTEM image of 12 nm Bi_2Se_3 on TmIG. Inset: Cs-corrected HAADF-STEM image showing the interface fine structure.

Fig. 4 (a) AHE signals were observed in 7 nm Bi_2Se_3 /TmIG structure from 70 K to 220 K; (b) FMR signals before (black) and after (blue and red) deposition of Bi_2Se_3 on TmIG with the SBLT growth.

Fig. 1

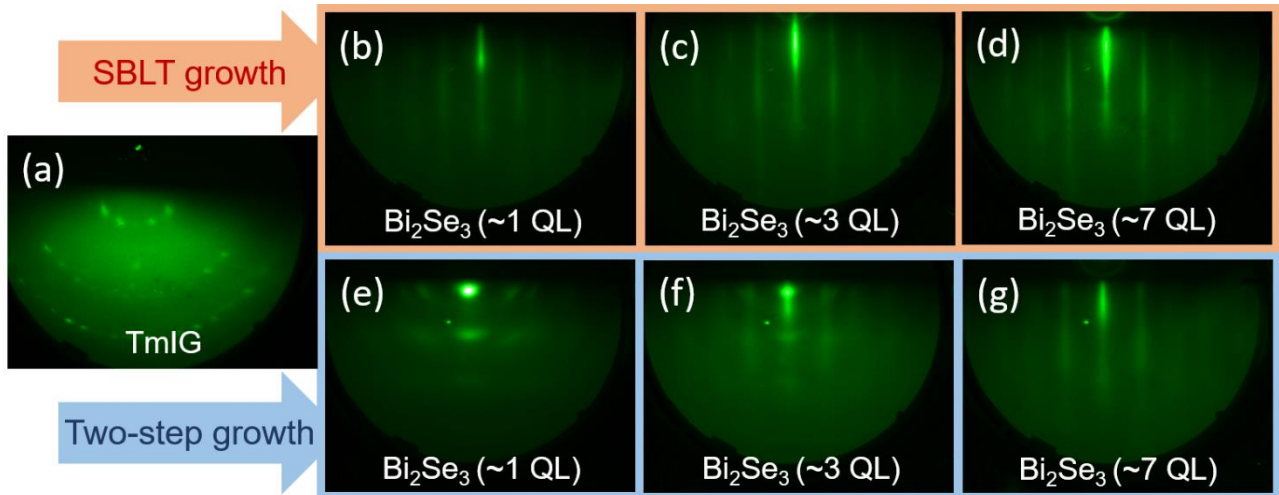


Fig. 2

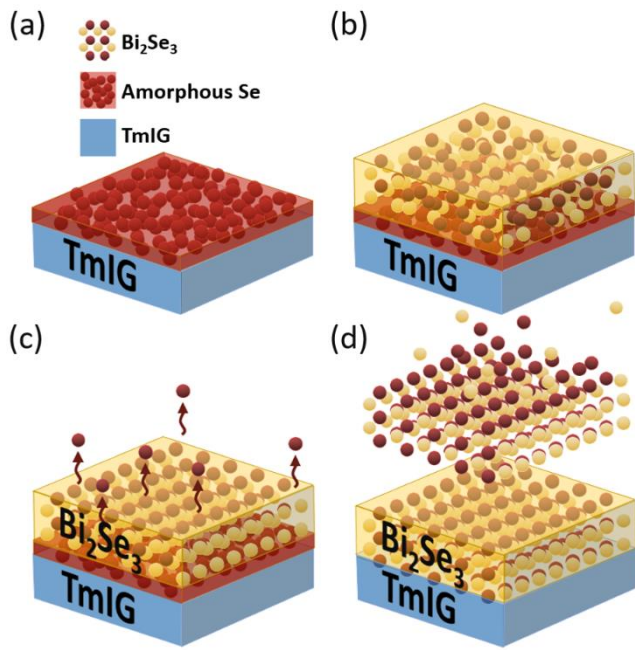


Fig. 3

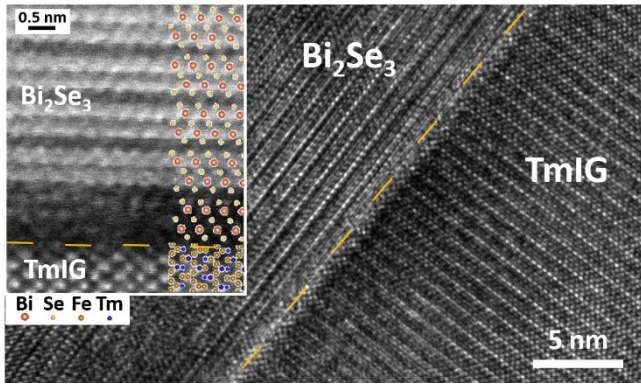


Fig. 4

